Effects of Heat Treatments on Microstructure Formation in MgB_2/YSZ/Hastelloy Film

Satoshi Hata, Harini Sosiati, Noriyuki Kuwano, Yoshitsugu Tomokiyo, Akiyoshi Matsumoto, Masao Fukutomi, Hitoshi Kitaguchi, Kazunori Komori, and Hiroaki Kumakura

***Abstract*—Annealing processes in MgB_2 films deposited on yttria-stabilized zirconia (YSZ)-buffered Hastelloy substrates were studied by transmission electron microscopy. The MgB_2 films with Mg-rich compositions were fabricated at room temperature using a pulsed laser deposition (PLD) method. The as-deposited films do not exhibit clear superconducting transitions, and have inhomogeneous microstructures composed of amorphous regions and a small amount of crystalline MgB_2 and MgO with several tens of nm in size. Various sizes of voids are also incorporated within the amorphous regions. After the annealing at 600 or 680°C, the films exhibit clear superconducting transitions. The amorphous regions crystallize into fine grains of MgB_2 or MgO 5–50 nm in size. The voids remain in the annealed films and their sizes depend on the annealing condition. Magnesium-and oxygen-rich layers are formed near the MgB_2/YSZ interface and the film surface. It is suggested that the finer grains of MgB_2 and MgO obtained by the lower-temperature annealing give a larger critical current density under a high magnetic field.**

***Index Terms*—Heat treatment, MgB_2 film, transmission electron microscopy, yttria-stabilized zirconia.**

I. Introduction

THE MgB_2 film is a potential material from a viewpoint of an application to superconducting electronic devices. Many research groups make efforts to produce high-quality MgB_2 films. It is known that MgB_2 films after an appropriate heat treatment show good superconducting properties [1]–[5]. The fact suggests that the heat treatment plays a significant role in improving the superconducting properties. The improvement of superconducting properties will be strongly correlated with the refinement of microstructure in MgB_2 films. However, the microstructure evolution in MgB_2 films during the heat treatment has not been intensively studied in comparison with the superconducting properties.

The present paper reports annealing effects on microstructures in MgB_2 films that were deposited on yttria-stabilized zirconia (YSZ)-buffered Hastelloy substrates using a pulsed laser deposition (PLD) method. The MgB_2/YSZ/Hastelloy films exhibit a high critical current density, J_c, under high magnetic fields after annealing treatments [6]. In the present study, transmission electron microscopy (TEM) analysis was carried out to clarify the microstructure evolution and its relation with the superconductivity in the MgB_2/YSZ/Hastelloy films.

Manuscript received October 4, 2004. This work was supported in part by Nanotechnology Support Project of the Ministry of Education, Culture, Sport, Science, and Technology, Japan.

S. Hata and Y. Tomokiyo are with the ASEM, Kyushu University, Kasuga 816-8580, Japan (e-mail: hata@asem.kyushu-u.ac.jp).

H. Sosiati is with the HVEM, Kyushu University, Fukuoka 812-8581, Japan.

N. Kuwano is with the ASTEC, Kyushu University, Kasuga 816-8580, Japan.

A. Matsumoto, M. Fukutomi, H. Kitaguchi, K. Komori, and H. Kumakura are with the National Institute for Materials Science, Tsukuba 305-0047, Japan.

Digital Object Identifier 10.1109/TASC.2005.848834

II. Experimental

A substrate of Hastelloy (C-276) tape was precoated with YSZ of 500 nm in thickness by bias sputtering [6]. MgB_2 and magnesium powders were mixed together so that the molar ratio of Mg to B was set to 3:2. The mixed powders were compacted to form a pellet used as a target material. By using a KrF excimer laser with 400 mJ/pulse operated at 5 Hz, Mg-rich MgB_2 films about 800 nm in thickness were deposited on the YSZ/Hastelloy substrates. The deposition was carried out at room temperature under an Ar atmosphere about 10^{-3} Pa. The as-deposited films were annealed at 600°C for 1 h or at 680°C for 0.5 h under an Ar atmosphere by heating the substrates. After the annealing, the thickness of the MgB_2 film reduced to 400–500 nm.

The critical current, I_c, was measured at 4.2 K under a magnetic field using a four-probe resistivity technique. The magnetic field was applied parallel to the film surface. The criterion of I_c determination was 1.0 $\mu V/cm$. The value of J_c was calculated by dividing the I_c value by the cross-sectional area of the MgB_2 film.

Cross-sectional specimens of the MgB_2/YSZ/Hastelloy films were prepared using a HITACHI FB-2000K focused ion beam mill equipped with a microsampling system. TEM observation of the specimens was performed with FEI TECNAI-20, TECNAI-20F and JEOL JEM-2010FEF electron microscopes. For the post-annealed MgB_2/YSZ/Hastelloy films, two-dimensional distribution of magnesium, boron and oxygen was analyzed using electron energy loss spectroscopy (EELS) and scanning TEM-energy dispersive X-ray spectroscopy (STEM-EDX) techniques. In the EELS experiment, the three-window technique was adopted and the magnesium-L edge at 55 eV, the boron-K edge at 188 eV and the oxygen-K edge at 532 eV were selected for imaging the elemental distribution. In the STEM-EDX experiment, the electron probe 1–3 nm in diameter was positioned on the specimen surface, and an EDX spectrum was acquired for 1–3 s at each position.

III. Results and Discussion

A. Superconducting Properties

The as-grown MgB_2/YSZ/Hastelloy films do not exhibit clear superconducting transitions. After the annealing at 600 or 680°C, however, the films exhibit superconducting

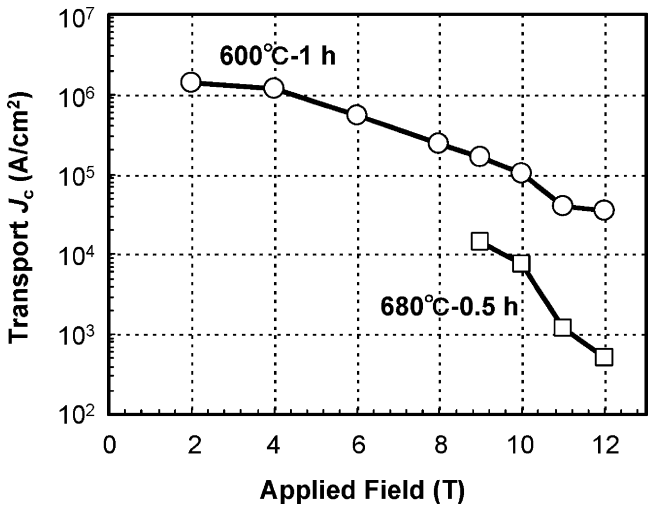

Fig. 1. Transport J_c at 4.2 K of MgB_2/YSZ/Hastelloy films after different heat treatments as a function of applied magnetic fields.

transitions at 30 K or 32 K, respectively. Fig. 1 shows transport J_c values of the post-annealed films as a function of applied magnetic fields. The J_c value of the film annealed at 600°C reaches 1.0×10^5 A/cm^2 at 10 T and decreases gradually with increasing magnetic fields. The J_c value of the film annealed at 680°C, on the other hand, decreases rapidly under higher magnetic fields. This suggests that the pinning force under high magnetic fields is higher in the 600°C-annealed film than in the 680°C-annealed one.

B. TEM Observation

Fig. 2(a) shows a bright-field TEM image of the as-deposited MgB_2 film. The as-deposited film has an inhomogeneous microstructure. Electron diffraction experiments revealed that the matrix of the deposited film is amorphous. Various sizes of voids are formed in the amorphous layer, as indicated by arrows. The electron diffraction pattern in (c) was taken from the encircled area in (a). Bragg reflections are indexed as those for MgB_2 and/or MgO phases. Fig. 2(b) shows a dark-field image taken with the reflections at $hkl = 101_{MgB2}$ and/or 200_{MgO}. Crystalline MgB_2 and MgO with tens of nm in size are inhomogeneously distributed within the amorphous layer.

Crystallization of MgB_2 and MgO occurred in the as-deposited film during the heat treatments. Fig. 3(a) shows a bright-field image of the 600°C-annealed film. Two different granular contrasts are seen in the MgB_2 film: one is a bright contrast of voids 5–50 nm in size and the other is a dark one of fine crystals 5–20 nm in size, as indicated by white and black arrows respectively. The electron diffraction in Fig. 3(c) shows clear diffraction rings from the MgB_2 and MgO phases. The dark-field image in Fig. 3(b) reveals that nanocrystalline MgB_2 and MgO are uniformly dispersed in the film.

The crystallization is also seen in a high-resolution TEM image in Fig. 4. High density of lattice fringes and grain connectivity are visible. Some lattice fringes were identified as those of MgB_2 and MgO by Fourier transformation analysis. No clear difference in grain size between MgB_2 and MgO was recognized. The existence of the grain connectivity suggests

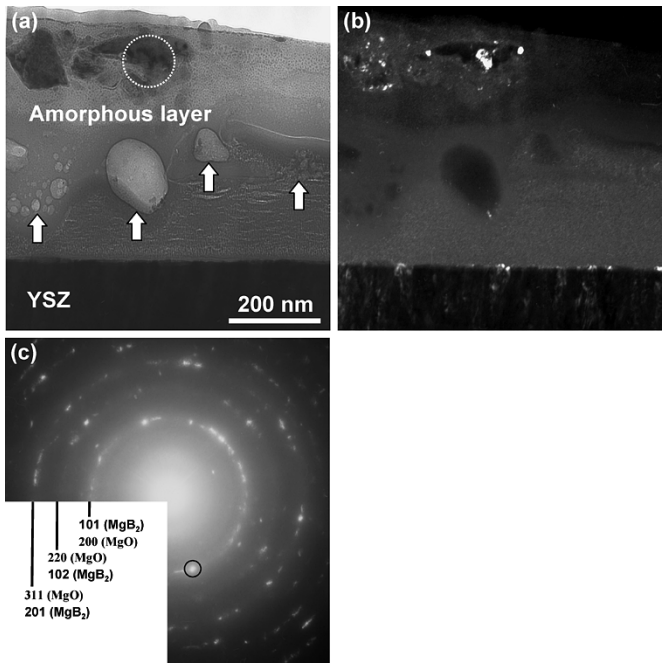

Fig. 2. (a) Bright- and (b) dark-field TEM images of the as-deposited film and an electron diffraction pattern (c) taken from the encircled area in (a). Various sizes of voids are formed as indicated by arrows in (a). Bragg reflections of $hkl = 101_{MgB2}$ and/or 200_{MgO} was used for the dark-field imaging, as depicted by a small circle in (c).

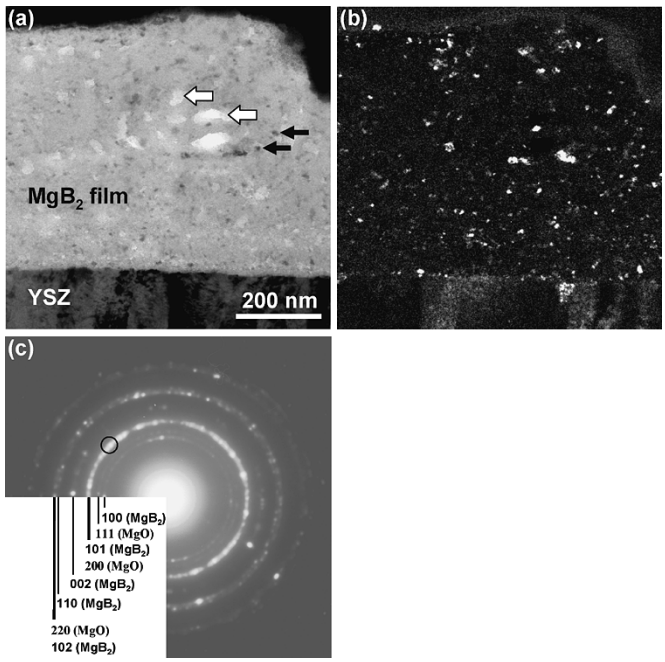

Fig. 3. (a) Bright- and (b) dark-field TEM images of the MgB_2 film annealed at 600°C for 1 h, and an electron diffraction pattern taken from the MgB_2 film (c). White and black arrows in (a) indicate voids and grains of MgB_2 or MgO, respectively. Bragg reflections of $hkl = 101_{MgB2}$ and 200_{MgO} was used for the dark-field imaging, as depicted by a small circle in (c).

that supercurrents would easily flow across the grain boundaries in the film. The voids show an amorphous-like contrast and it changed every moment during the observation. This suggests that some unknown phases, which may be oxide phases, exist in the voids.

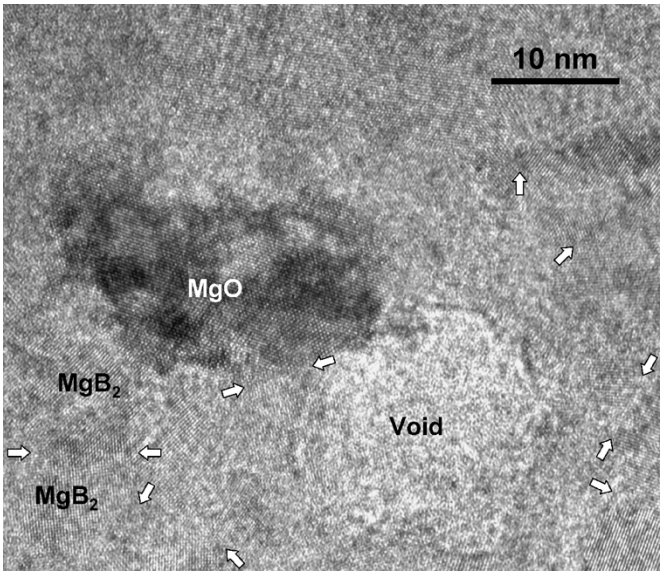

Fig. 4. High-resolution TEM images of the MgB_2 film annealed at 600°C for 1 h. Grains of MgB_2 and/or MgO are in contact with each other, as indicated by arrows.

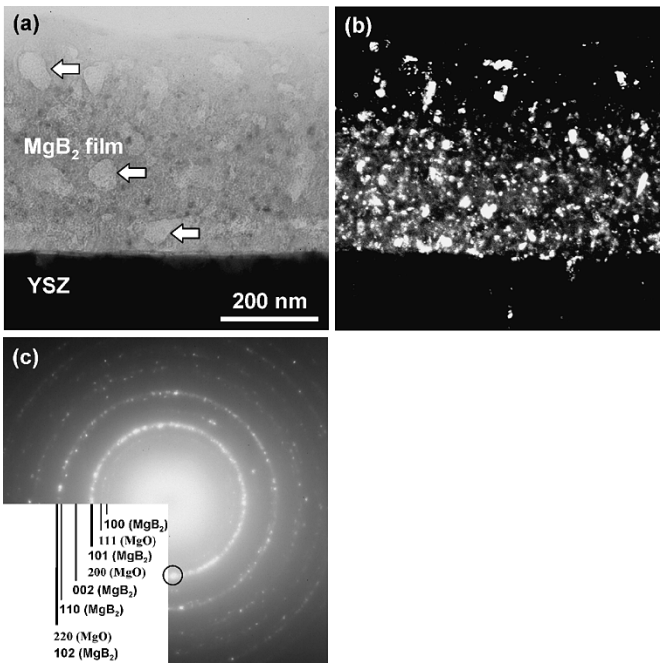

Fig. 5. (a) Bright- and (b) dark-field TEM images of the MgB_2 film annealed at 680°C for 0.5 h, and an electron diffraction pattern taken from the MgB_2 film (c). Arrows in (a) indicate large voids. Bragg reflections of $hkl = 101_{MgB2}$ and 200_{MgO} was used for the dark-field imaging, as depicted by a small circle in (c).

Fig. 5 shows TEM results of the 680°C-annealed film. Bright-(a) and dark-field images (b) clearly show that both voids and grains of MgB_2 and MgO are larger in size than those in the 600°C-annealed film. Diffraction intensities from the MgB_2 phase in Fig. 5(c) tend to be higher than those for the 600°C-annealed film. This corresponds to the larger grain sizes of MgB_2. The higher crystallinity of MgB_2 might be also correlated with the larger diffraction intensities in the 680°C-annealed film.

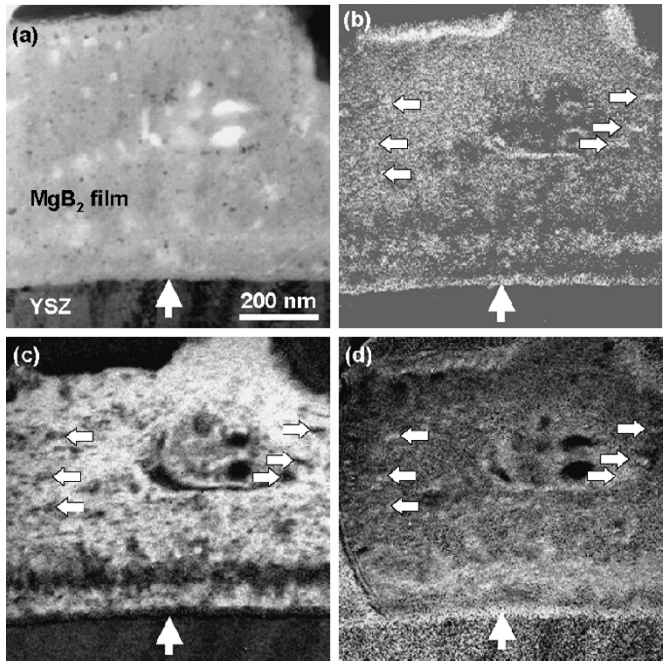

Fig. 6. EELS mapping of the MgB_2 film annealed at 600°C for 1 h. (a) Bright-field image, (b) Magnesium map, (c) boron map and (d) oxygen map. Large and small arrows indicate the MgB_2/YSZ interface and grains of MgO, respectively.

C. Elemental Mapping Analysis

Fig. 6 demonstrates an EELS mapping analysis of the 600°C-annealed film. Large arrows indicate the MgB_2/YSZ interface. One can see that the distribution of oxygen (d) is similar to that of magnesium (b), and boron (c) tends to exhibit the reverse distribution. Such elemental distribution may be due to the high reactivity of magnesium with oxygen and the excess magnesium content in the MgB_2 film. The magnesium and oxygen concentrations are significantly high at (i) the film surface, (ii) small areas in the film as indicated by small arrows and (iii) the MgB_2/YSZ interface. The enrichment of magnesium and oxygen occurs during the heat treatment, and enrichment processes can be explained respectively as follows: (i) the reaction of magnesium at the film surface with residual oxygen in the atmosphere, (ii) the formation of nano-crystalline MgO in the film and (iii) the reaction of magnesium with oxygen coming from the YSZ layer. A close observation of the MgB_2 film near the MgB_2/YSZ interface reveals that the (Mg,O)-rich layers and B-rich layers are formed alternately. The formation of such a 'layered structure' may be related to the directional heating from the substrate toward the MgB_2 film.

Fig. 7(a) shows a STEM-EDX result of the 600°C-annealed film. The graph depicts profiles of characteristic X-ray intensities measured along the dotted line in the annular dark-field STEM image. One can see that zirconium and yttrium do not diffuse into the MgB_2 layer. The X-ray intensities of magnesium and oxygen exhibit some maxima near the MgB_2/YSZ interface. These intensity maxima correspond to the layered structure identified in the EELS mapping. At the large voids, the magnesium intensity decreases rapidly whereas the oxygen intensity does not, as indicated by the circle in the graph. This sug-

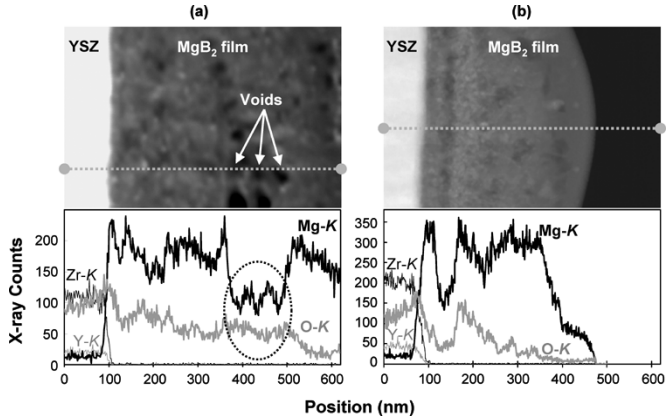

Fig. 7. STEM-EDX analysis of the 600°C- (a) and 680°C-annealed films (b). Characteristic X-ray intensities were measured along the dotted lines depicted in the annular dark-field STEM images.

gests that some oxide phases exist inside the voids. The semi-quantitative STEM-EDX analysis in Fig. 7 also revealed differences in elemental distribution between the 600°C- (a) and 680°C-annealed films (b). The condensation of magnesium and oxygen near the MgB_2/YSZ interface is more remarkable in the 680°C-annealed film (b). On the other hand, the oxygen concentration in the MgB_2 matrix tends to be higher in the 600°C-annealed film (a) than in 680°C-annealed one (b).

D. Relationship Between Microstructure and J_c Property

Control of the grain size of MgB_2 is important to improve the J_c property of the MgB_2 film, since grain boundaries are considered as effective pinning centers in the MgB_2 film. In the present study, the 600°C-annealed film exhibits smaller grain sizes (higher grain boundary density) of MgB_2 and a better J_c property under high magnetic fields. This suggests that the lower-temperature annealing is effectual to fabricate high-J_c MgB_2 films.

In the PLD process, nano-sized voids were introduced in the MgB_2 films. Such void formation in the PLD-MgB_2 films was also reported by other research groups [7]. The voids remain after the annealing and contain oxygen-rich phases. We also found that high density of nano-sized voids exist in the (Mg,O)-rich layers near the MgB_2/YSZ interface. These results suggest that the void formation is closely related to the reaction of oxygen as well as the PLD process. The size of voids depends on the annealing temperature. The large-void formation in the 680°C-annealed film may be due to (i) the coalescence of voids during the annealing or (ii) the coarsening of voids with incorporating oxygen from neighboring oxide phases, such as MgO and $Mg(B,O)_2$. For the 600°C-annealing, on the other hand, oxygen atoms cannot diffuse away from the MgB_2 matrix, but form a significant amount of oxide phases. As a result, the oxygen concentration in the MgB_2 matrix of the 600°C-annealed film becomes higher than that in the 680°C-annealed film, as seen in Fig. 7. Although no direct evidence for the formation of oxide phases other than MgO, some of nano-crystalline MgB_2 might exist as $Mg(B,O)_2$ in the 600°C-annealed film. Such oxide phases are also considered to act as pinning centers when their grain sizes are smaller than 10–20 nm [2], [5]–[11]. There is another possibility that the nano-sized oxide phases may suppress the grain growth of nanocrystalline MgB_2. Thus, control of the nanostructure formation of oxide phases in the heat treatments is also important to fabricate high-J_c MgB_2 films.

REFERENCES

[1] W. N. Kang, H.-J. Kim, E.-M. Choi, C. U. Jung, and S.-I. Lee, "MgB_2 superconducting thin films with a transition temperature of 39 Kelvin," *Science*, vol. 292, pp. 1521–1523, 2001.

[2] C. B. Eom *et al.*, "High critical current density and enhanced irreversibility field in superconducting MgB_2 thin films," *Nature*, vol. 411, pp. 558–560, 2001.

[3] Y. Zhao, M. Ionescu, A. V. Pan, S. X. Dou, and E. W. Collings, "*In situ* annealing of superconducting MgB_2 films prepared by pulsed laser deposition," *Supercond. Sci. Technol.*, vol. 16, pp. 1487–1492, 2003.

[4] Z. Mori *et al.*, "Two-step *in situ* annealing effects on sputter-deposited MgB_2 thin films," *Supercond. Sci. Technol.*, vol. 17, pp. 47–50, 2004.

[5] M. Naito and K. Ueda, "MgB_2 thin films for superconducting electronics," *Supercond. Sci. Technol.*, vol. 17, pp. R1–R18, 2004.

[6] K. Komori *et al.*, "Approach for the fabrication of MgB_2 superconducting tape with large in-field transport critical current density," *Appl. Phys. Lett.*, vol. 81, pp. 1047–1049, 2002.

[7] X. X. Xi *et al.*, "Thermodynamics and thin film deposition of MgB_2 superconductors," *Supercond. Sci. Technol.*, vol. 15, pp. 451–457, 2002.

[8] D. Eyidi *et al.*, "Superconducting properties, microstructure and chemical composition of MgB_2 sheathed materials," *Supercond. Sci. Technol.*, vol. 16, pp. 778–788, 2003.

[9] X. Z. Liao *et al.*, "$Mg(B,O)_2$ precipitation in MgB_2," *J. Appl. Phys.*, vol. 93, pp. 6208–6215, 2003.

[10] R. F. Klie *et al.*, "Direct observation of nanometer-scale Mg-and B-oxide phases at grain boundaries in MgB_2," *Appl. Phys. Lett.*, vol. 79, pp. 1837–1839, 2002.

[11] ——, "Observation of coherent oxide precipitates in polycrystalline MgB_2," *Appl. Phys. Lett.*, vol. 80, pp. 3970–3972, 2002.